Temporal fluctuations in the bosonic Josephson junction as a probe for phase space tomography

Christine Khripkov[1], Doron Cohen[2], and Amichay Vardi[1]
Departments of [1]Chemistry and [2]Physics, Ben-Gurion University of the Negev, Beer-Sheva 84105, Israel

We study the long time coherence dynamics of a two-mode Bose-Hubbard model in the Josephson interaction regime, as a function of the relative phase and occupation imbalance of an arbitrary coherent preparation. We find that the variance of the long time fluctuations of the one-body coherence can be factorized as a product of the inverse participation number $1/M$ that depends only on the preparation, and a semi-classical function $C(E)$ that reflects the phase space characteristics of the pertinent observable. Temporal fluctuations can thus be used as a sensitive probe for phase space tomography of quantum many-body states.

The two mode Bose-Hubbard Hamiltonian (BHH) appears in different guises in a perplexing variety of fields. Cast in spin form, it is known in nuclear physics as the Lipkin-Meshkov-Glick (LMG) model of shape phase transitions [1]. It is broadly used to describe interacting spin systems [2] and serves as a paradigm for squeezing and entanglement [3]. As such, it offers schemes for the generation of squeezed states for optical interferometry below the standard quantum limit [4], and its matter-wave equivalent [5]. It is commonly employed to describe the Josephson dynamics in systems of bosonic atoms in double-well potentials [6] and suggests prospects for the generation of macroscopic superposition states [7]. The same model is also known in condensed matter physics as the integrable dimer model [8] with applications to the dynamics of small molecules, molecular crystals, and self-trapping in amorphous semiconductors.

Like the paradigmatic Jaynes-Cummings model in quantum optics [9], the bimodal BHH dynamics with a coherent spin state preparation exhibits a series of collapses and revivals of its single-particle coherence due to interactions [10–13]. These recurrences are manifested in the collapse and revival of the Rabi-Josephson population oscillations, or of the multi-realization fringe visibility, when the two condensates are released and allowed to interfere. Below we study the long time BHH dynamics for general coherent spin preparations $|\theta,\phi\rangle$. In such states all particles occupy a single superposition of the two modes, with a normalized population imbalance $S_z = \cos(\theta)$ and a relative phase ϕ.

The characteristics of this dephasing-rephasing dynamics strongly depend on the dimensionless interaction parameter $u = UN/K$, where U is the interaction strength, N is the total particle number, and K is the hopping amplitude. In the linear Rabi regime ($u < 1$) time evolution is straightforward because the interaction is weak and the nature of the dynamics is essentially single-particle. Accordingly, one observes only coherent Rabi oscillations in the population difference with a typical frequency $\omega_J \equiv \sqrt{K(K-UN)} = K\sqrt{1-u} \approx K$ which reflects mainly the coupling K between the two modes, accompanied by a slow loss of single particle coherence.

The coherence dynamics in the highly nonlinear Fock regime ($u > N^2$) are also fairly simple because it reflects the Fock basis expansion of the initial coherent preparation. For such strong interactions the two-mode BHH generates precisely the same coherence dynamics as the many-mode BHH of a BEC in an optical lattice, because the local modes are essentially decoupled, hence the dynamics is fully captured by the Gutzwiller ansatz of a direct product of single-site states, each of which is a coherent wavepacket of number states [14, 15, 18, 19]. This allows for monitoring the fringe visibility in single shot interferometery of an optical lattice, rather than repeating a two-mode experiment many times. The expected coherence recurrences have been observed experimentally for optical lattices with relatively small occupation numbers [14, 15] with a striking demonstration of exceptionally long time dynamics, allowing to probe effective multi-body interactions through the dependence of U on the number of atoms [16].

The dynamics in the Josephson regime ($1 < u < N^2$) is by far richer and more intricate, reflecting the coexistence of three distinct phase space regions [11, 12]. Unlike the Fock-space recurrences which only depend on the population imbalance, the Josephson coherence dynamics is also highly sensitive to the relative phase. Previous work has considered specific preparations that were of contemporary experimental relevance, e.g. small perturbation of the ground state that results in Josephson oscillations, or a large population imbalance that leads to self-trapping [17]. Here we adopt a global, tomographic approach by characterizing the long time temporal quantum fluctuations for *all* possible coherent preparations. This appears to be a formidable task, but as shown below, a relatively simple semi-classical perspective provides an adequate framework for the required analysis.

The BHH.– We consider a similar scenario to that in Ref. [15], which observed the long time collapse and revival of coherence in the Fock regime. In the Josephson regime, the dynamics of a lattice with one mode per site is quite different from the two-mode dynamics. However, the two-mode model can be realized with two spin components in each isolated site [20] or with an array of independent double wells [21], thus retaining the convenience of single-shot measurements. We note recent work on BECs in 1D double-well traps reporting the breakdown

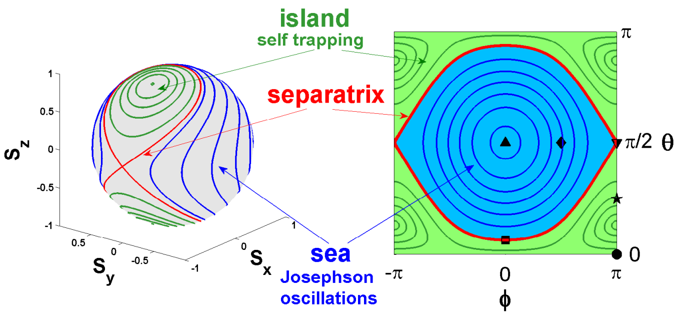

FIG. 1: (color online) Phase-space structure of the bosonic Josephson junction in the Josephson regime ($u = 2.5$). Lines depict equal energy contours, i.e. classical trajectories. A separatrix trajectory with an isolated hyperbolic point at $(\theta, \phi) = (\pi/2, \pi)$ separates Rabi-Josephson oscillations around the ground state in a K-dominated 'sea' from nonlinear self-trapped phase-oscillations in two high-energy 'islands'. Symbols denote the coherent preparations used in Fig. 2.

of the lowest Bloch band BHH model at interaction parameter values as low as $u = 2.15$ for this realization [22, 23].

Assuming that no bias field is applied, the pertinent BHH is,

$$\begin{aligned} \mathcal{H} &= -\frac{K}{2}\left(\hat{a}_1^\dagger \hat{a}_2 + \hat{a}_2^\dagger \hat{a}_1\right) \\ &+ \frac{U}{2}\left[\hat{n}_1\left(\hat{n}_1 - 1\right) + \hat{n}_2\left(\hat{n}_2 - 1\right)\right], \qquad (1) \end{aligned}$$

where $\hat{a}_i$ and $\hat{a}_i^\dagger$ are bosonic annihilation and creation operators, respectively. The particle number operator in mode i is $\hat{n}_i = \hat{a}_i^\dagger \hat{a}_i$. Since the total particle number $\hat{n}_1 + \hat{n}_2 = N$ is conserved, we can eliminate respective c-number terms and obtain the BHH in spin form,

$$\hat{H} = -K\hat{J}_x + U\hat{J}_z^2 , \qquad (2)$$

where $\hat{J}_x = (\hat{a}_1^\dagger \hat{a}_2 + \hat{a}_2^\dagger \hat{a}_1)/2$, $\hat{J}_y = (\hat{a}_1^\dagger \hat{a}_2 - \hat{a}_2^\dagger \hat{a}_1)/(2i)$, and $\hat{J}_z = (\hat{n}_1 - \hat{n}_2)/2$. The number conservation becomes angular momentum conservation with $j = N/2$. Below we assume for simplicity that the interaction is repulsive $U > 0$, but the $U < 0$ case (to the extent that the particle number is sufficiently small that the attractive BEC is stable) amounts to a simple transformation $K \mapsto -K$, and $E \mapsto -E$. Thus the phase space with attractive interaction is simply an inverted mirror image of the repulsive-interaction case and there is no loss of generality. In this spin representation, each state is characterized by the normalized Bloch vector $\mathbf{S} \equiv \langle \mathbf{J} \rangle / j$, where its z projection $S_z = \cos(\theta)$ corresponds to the normalized population imbalance, its azimuthal angle ϕ corresponds to the relative phase between the modes, and its length S corresponds to the single-particle coherence.

The classical phase space structure of the BHH is set by the previously defined dimensionless interaction parameter u. Its characteristics in the three interaction regimes are discussed in great detail elsewhere [6, 11, 12]. In Fig. 1 we plot the equal-energy contour lines and the pertinent phase-space regions in the Josephson regime ($1 < u < N^2$). Two nonlinear islands are separated from a nearly-linear sea region by a separatrix trajectory. The sea trajectories correspond to Rabi-Josephson population oscillations around the ground state, whereas the island trajectories correspond to self-trapped phase-oscillations [17]. In the Fock regime ($u > N^2$) the sea becomes too small to support quantum states, while in the opposite limit - in the Rabi regime ($u < 1$) - the islands disappear, so that only Rabi-type oscillations are feasible.

Evolution.– We study the dynamics induced by the Hamiltonian of Eq. (2), starting from an arbitrary spin coherent state preparation,

$$\begin{aligned} |\theta, \phi\rangle &\equiv \frac{1}{N!}\left[\cos(\theta/2)\hat{a}_1^\dagger + \sin(\theta/2)e^{i\phi}\hat{a}_2^\dagger\right]^N |\text{vac}\rangle \\ &= \exp(-i\phi\hat{J}_z)\exp(-i\theta\hat{J}_y)|J_z = j\rangle, \qquad (3) \end{aligned}$$

where $|\text{vac}\rangle$ and $|J_z = j\rangle$ are the vacuum states of the Heisenberg-Weil and SU(2) algebras, respectively. The preparation of such arbitrary coherent states can be attained via a two step process as implied by Eq. (3) and demonstrated experimentally in Ref. [24], in which θ is set by a coupling pulse and ϕ by a bias pulse. We focus our attention on experimentally relevant observables such as the population imbalance S_z and the single-particle coherence S. Note that S is the best fringe visibility one may expect to measure by proper manipulation of the Bloch vector, i.e. if we are allowed to perform any SU(2) rotation. The expected fringe visibility if interferometry is carried out without further manipulation is $g_{12}^{(1)} = (1/j)[|\langle \hat{J}_x \rangle|^2 + |\langle \hat{J}_y \rangle|^2]^{1/2}$. For presentation purpose we focus on S, but the results for $g_{12}^{(1)}$ are very similar.

The intricacy of the Josephson regime quantum dynamics is illustrated in Fig. 2, where we plot the full quantum evolution under the BHH (2), of the population imbalance and of the one-particle coherence for several representative coherent preparations (corresponding to the symbols in Fig. 1). It is clear that different preparations lead to qualitatively different behavior, depending on the initial population imbalance and on the relative phase. Moreover, different preparations located on the same classical trajectory produce dramatically different recurrence patterns (see e.g. the differences in the coherence dynamics between the two on-separatrix preparations marked by square and inverted triangle in Fig. 2b). The cause of this diversity is that different coherent preparations sample different parts of the spectrum. Each coherent spin state constitutes a superposition of eigenstates that can be associated with qualitatively different regions in the corresponding classical phase space. This is in a stark contrast to the Rabi and Fock regimes, where the eigenstates occupy, so to say, a single component phase space that allows only one type of motion.

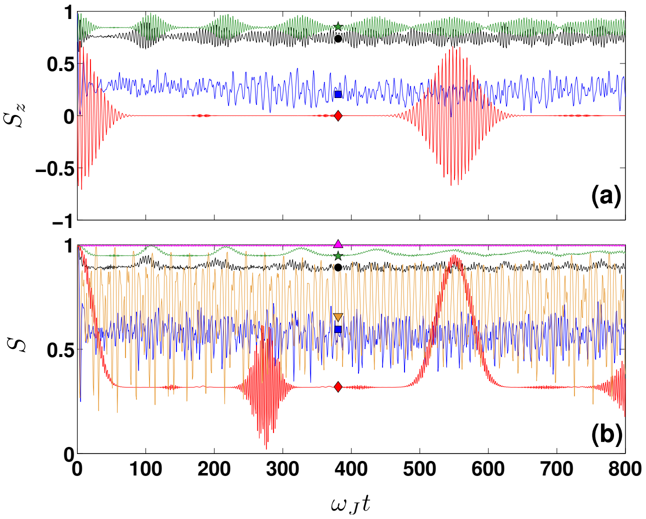

FIG. 2: (color online) Collapse and revival dynamics of the normalized population imbalance S_z (top) and of the single-particle coherence S (bottom) for the representative coherent preparations marked in Fig. 1. The BHH parameters here and in all subsequent figures are $N = 100$ and $u = 2.5$, corresponding to the Josephson regime.

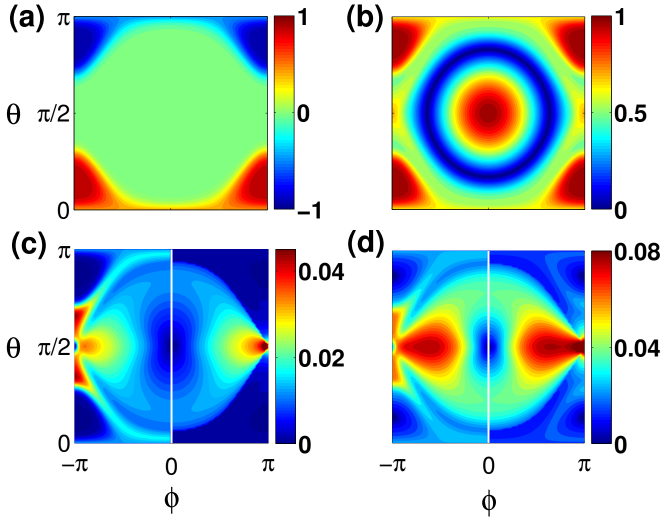

FIG. 3: (color online) (a) Long time average of the population imbalance $S_z(t)$, (b) Long time average of the one-particle coherence $S(t)$, (c) variance of $S_z(t)$, (d) variance of $S(t)$, all starting from arbitrary coherent preparations $|\theta, \phi\rangle$. The left side of panels c,d correspond to the numerical results which are the same as Eq. (5) whereas the right side is the factorization of Eq. (6).

For each preparation $|\theta, \phi\rangle$ we characterize the temporal fluctuations of the expectation values $A(t) = \langle \hat{A} \rangle_t$ of the pertinent observables, by their time-average $\overline{A(t)}$ and by their variance $\sigma_A^2 \equiv \overline{A^2(t)} - \overline{A(t)}^2$ taken over long times compared to the collapse and revival timescale. In order to see the overall picture, we plot in Fig. 3 an image of $\overline{S}_z(\theta, \phi)$, $\overline{S}(\theta, \phi)$, $\sigma^2_{S_z}(\theta, \phi)$, and $\sigma^2_S(\theta, \phi)$ for all the possible coherent preparations $|\theta, \phi\rangle$.

The $\overline{S}_z(\theta, \phi)$ average in Fig. 3a is straightforward to understand in classical terms. Sea trajectories have zero average population imbalance, whereas self-trapped island trajectories retain a finite imbalance. Note that the formal infinite-time average of the population imbalance is identically zero also for island preparations, due to the definite mode-exchange parity of energy eigenstates implying the many-body tunneling between islands. However, the N-particle tunnel splitting of the odd and even catlike eigenstates constituting a localized island preparation, is *exponentially small* in N. Therefore this formal observation is of no physical relevance, e.g. in our simulations here it corresponds to no less than 10^{13} Josephson periods before localization is lost. It should thus be understood that 'long time average' is still carried over a much shorter time than the N-particle tunneling time.

The imbalance fluctuations (Fig. 3c) show a far more complex structure which does not seem to be directly related to the mean-field trajectories. Similarly, the average and fluctuations of the single-particle coherence (Fig. 3b,d) can not be attributed to classical features alone. Below we analyze and explain these observed patterns, showing that they are the product of distinct quantum and semiclassical factors.

Analysis.– In order to deduce the exact time average of any $A(t)$, we expand it in the energy basis as

$$A(t) \;=\; \sum_{\nu,\mu} c^*_\nu c_\mu A_{\nu\mu} \exp[(E_\nu - E_\mu)t/\hbar], \qquad (4)$$

where $|E_\nu\rangle$ are the BHH eigenstates, $c_\nu = \langle E_\nu|\psi\rangle$ are the expansion coefficients of the initial state $|\psi\rangle = |\theta, \phi\rangle$, and $A_{\nu\mu} = \langle E_\nu|\hat{A}|E_\mu\rangle$. The long-time average eliminates the oscillating terms, hence $\overline{A(t)} = \sum_\nu p_\nu A_{\nu\nu}$, with probabilities $p_\nu \equiv |c_\nu|^2$, while the variance is

$$\sigma_A^2 \;=\; \sum_{\nu\neq\mu} p_\nu p_\mu |A_{\nu\mu}|^2 \; . \qquad (5)$$

The matrix elements in Eq.(5) can be evaluated semiclassically using the following prescription [12, 25]: a classical trajectory of energy E is generated using the BHH mean field equations of motion, and $A_{cl}(t)$ is calculated; then the classical power-spectrum $\tilde{C}^{cl}_A(\omega)$ is obtained via a Fourier transform of $[A_{cl}(t) - \overline{A_{cl}}]$; and finally the result is divided by the mean level spacing ϱ at that energy, providing the approximation $|A_{\nu\mu}|^2 \approx \tilde{C}^{cl}_A(E_\nu - E_\mu)/(2\pi\varrho)$. This is a very general procedure which is usually applied to chaotic systems, but it applies equally well to the integrable non-linear motion of the two-mode BHH. The number of eigenstates that contribute to Eq. (5), is conventionally evaluated as the *participation number* $M \equiv [\sum_\nu p_\nu^2]^{-1}$. Assuming $M \gg 1$, approximating $p_\nu \approx 1/M$, and neglecting non-participating eigenstates, we obtain that,

$$\sigma_A^2 = \frac{1}{M} C_A(E), \qquad (6)$$

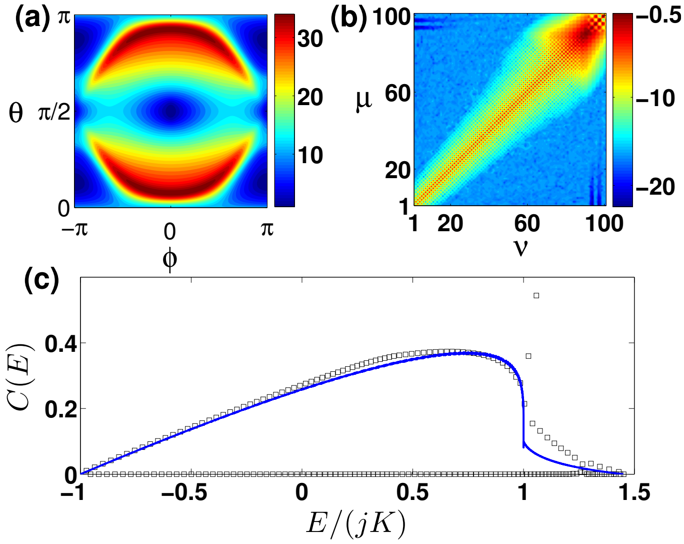

FIG. 4: (color online) (a) The participation number $M(\theta, \phi)$ for all coherent preparations $|\theta, \phi\rangle$ (b) image of the matrix elements $|A_{nm}|$, with color-scale in log10 units; (c) The power spectrum $C_A(E)$, evaluated according to the middle (symbols) and the r.h.s. (lines) of Eq.(7). The separatrix energy is E/Kj=1.

where,

$$C_A(E) = \sum_{|r|>0} |A_{\nu\mu}|^2 = \int \tilde{C}_A^{cl}(\omega) \frac{d\omega}{2\pi}. \qquad (7)$$

Above $r = (\nu - \mu)$ is the diagonal coordinate of the matrix, and it is implicit that the summation is carried out over a section $\nu + \mu = \text{const}$ such that $(E_\nu + E_\mu)/2 \sim E$. Note that the time variation of $A_{cl}(t)$ is non-linear but periodic, accordingly the integral in Eq. (7) is related, up to a form factor, to the classical amplitude.

Equation (6) with the definition (7) constitutes our primary result in this work. Given any observable with a fluctuating expectation value that has long time average, its variance can be approximated accurately as a product of the quantum term $1/M$ and a semi-classical term $C_A(E)$, corresponding to the classical fluctuations of A along a mean-field trajectory that has an energy E. Below we show that indeed this factorization results in the apparently complex patterns of Fig. 3c,d.

Numerical verification.– The required ingredients for the calculation of the variance $\sigma_A^2(\theta, \phi)$ according to the semiclassical prescription, are shown Fig. 4 for the population imbalance $A = J_z$. In order to evaluate the variance of the fluctuations, we need to calculate the participation number M for a general coherent preparation $|\theta, \pi\rangle$. The result is shown in Fig. 4a. Due to the factorization Eq.(6), this function needs be calculated only once for all desired observables. While we do not have a closed analytic expression for $M(\theta, \phi)$, its characteristic value and its dependence on u and N in the different phase space regions can be evaluated from general considerations as detailed in Ref. [12]. Generally speaking, the highest participation numbers are obtained at the top of the separatrix and scale as $M \approx \sqrt{N} \log(N/u)$, i.e. like the square root of N. By contrast, the equatorial states $|\pi/2, 0\rangle$ and $|\pi/2, \pi\rangle$ have participation numbers of order unity: $M(\pi/2, 0) \approx \sqrt{u}$ and $M \approx \sqrt{u} \log(N/u)$, respectively.

The matrix elements $(J_z)_{\nu\mu}$ are shown in panel Fig. 4b, confirming the assumption of a broad spectrum containing many frequencies but within a narrow band from the main diagonal. The results of the summation over the matrix elements and the integration over the classical fluctuations to obtain the power spectrum $C_A(E)$ according to Eq.(7) are compared in panel Fig. 4c, showing good agreement except for a small region in the vicinity of the separatrix energy.

Similar calculations were carried out for the single-particle coherence and fringe visibility. On the right hand side of Fig. 3c and Fig. 3d we use the participation number M and the calculated power spectrum $C_A(E)$ to predict the variance of the population imbalance and coherence oscillations for the various preparations. Comparison to the results obtained by numerical propagation or by using Eq. (5) (left side of the same panels) shows good agreement and confirms the validity of Eq.(6). Similar agreement is obtained for the fringe visibility which is not shown here for lack of space.

The interpretation of the fluctuation patterns in panels c,d of Fig. 3 now becomes clear. Long time population oscillations will only survive in the vicinity of the unstable equal-population $\phi = \pi$ preparation, where the power spectrum is large and the participation number is small. Note that the classical fluctuations are large for the other separatrix preparations, too, but away from $\phi = \pi$ the participation number is large, and hence the quantum fluctuations are quenched. It should also be noted that our approximation breaks down in the vicinity of the hyperbolic point $(\theta, \phi) = (\pi/2, \pi)$ because the semiclassical assumption $M \gg 1$ is not satisfied.

Summary.– The magnitude of the long-time quantum fluctuations of an arbitrary observable A can be deduced from the tractable classical dynamics and from the a-priori known participation number of all coherent preparations. Moreover, because $C_A(E)$ only depends on energy, it is possible to obtain a tomographic image of the phase space from the observed fluctuations by plotting $M\sigma_A^2$. The contours of this plot trace the equal energy lines and their values are specific to the measured observable. Eq. (6) constitutes a dramatic reduction in complexity and offers great insight on the dynamics of the two-mode BHH. It is successfully employed above to characterize the observed fluctuations in population imbalance, one-particle coherence, and fringe-visibility.

Acknowledgments.– This research was supported by the Israel Science Foundation (grant Nos. 346/11 and 29/11) and by the United States-Israel Binational Science Foundation (BSF).

[1] H. J. Lipkin, N. Meshkov, and A. J. Glick, Nucl. Phys. **62**, 188 (1965); P. Ribeiro, J. Vidal, and R. Mosseri, Phys. Rev. Lett. **99**, 050402 (2007); P. Ribeiro, J. Vidal, and R. Mosseri, Phys. Rev. E **78**, 021106 (2008).

[2] R. Botet and R. Julien, Phys. Rev. B **28**, 3955 (1983).

[3] M. Kitagawa and M. Ueda, Phys. Rev. A **47**, 5138 (1993); A. Sorensen and K. Molmer, Phys. Rev. Lett. **86**, 4431 (2001); A. Sorensen, L. M. Duan, J. I. Cirac, and P. Zoller, Nature **409**, 63 (2001); A. Micheli, D. Jaksch, J. I. Cirac, and P. Zoller, Phys. Rev. A **67**, 013607(2003); C. Bodet, J. Esteve, M. K. Oberthaler, and T. Gasenzer, Phys. Rev. A **81**, 063605 (2010).

[4] C. M. Caves, Phys. Rev. D **23**, 1693 (1981); B. Yurke, S. L. McCall, and J. R. Klauder, Phys. Rev. A **33**, 4033 (1986); M. J. Holland and K. Burnett, Phys. Rev. Lett. **71**, 1355 (1993);

[5] C. Gross, T. Zibold, E. Nicklas, J. Esteve, and M. K. Oberthaler, Nature **464**, 7292 (2010); M. F. Riedel, P. Böhi, Y. Li, T. W. Hänsch, A. Sinatra, and P. Treutlein, Nature bf 464, 1170 (2010).

[6] A. V. Turbiner, Commn. Math. Phys. **118**, 467 (1988); V. V. Ulyanov and O. B. Zaslavskii, Phys. Rep. **216**, 179 (1992); A. Vardi and J. R. Anglin, Phys. Rev. Lett. **86**, 568 (2001); J. R. Anglin and A. Vardi, Phys. Rev. A **64**, 013605 (2001); M. Albiez *et al.*, Phys. Rev. Lett. **95**, 010402 (2005); R. Gati and M. Oberthaler, J. Phys. B **40**, R61 (2007);

[7] J. I. Cirac, M. Lewenstein, K. Molmer, and P. Zoller, Phys. Rev. A. **57**, 1208 (1998); T.-L Ho and C. V. Ciobanu, J. Low Temp. Phys. **135**, 257 (2004); Y. P. Huang and M. G. Moore, Phys. Rev. A. **73**, 023606 (2006).

[8] J. C. Eilbeck, P. S. Lomdahl, and A. C. Scott, Physica 16D, 318 (1985); L. Bernstein, J. C. Eilbeck, and A. C. Scott, Nonlinearity **3**, 293 (1990); S. Aubry, S. Flach, K. Klado, and E. Olbrich, Phys. Rev. Lett. **76**, 1607 (1996); G. Kalosakas and A. R. Bishop, Phys. Rev. A **65**, 043616 (2002).

[9] E.T. Jaynes, F.W. Cummings, Proc. IEEE **51**, 89 (1963); F.W. Cummings, Phys. Rev. **140**, A1051 (1965); J.H. Eberly, N.B. Narozhny, and J.J. Sanchez-Mondragon, Phys. Rev. Lett. **44**, 1323 (1980).

[10] G. J. Milburn, J. Corney, E. M. Wright, and D. F. Walls, Phys. Rev. A **55**, 4318 (1997); A. Imamoglu, M. Lewenstein, and L. You, Phys. Rev. Lett. **78**, 2511 (1997); G. Kalosakas, A. R. Bishop, and V. M. Kenkre, Phys. Rev. A **68**, 023602 (2003); K. Pawlowski, P. Zin, K. Rzazewski, and M. Trippenbach, Phys. Rev. A **83**, 033606 (2011).

[11] E. Boukobza, M. Chuchem, D. Cohen, and A. Vardi, Phys. Rev. Lett. **102**, 180403 (2009).

[12] M. Chuchem, K. Smith-Mannschott, M. Hiller, T. Kottos, A. Vardi, and D. Cohen, Phys. Rev. A **82**, 053617(2010).

[13] M. Egorov *et al.*, Phys. Rev. A **84**, 21605(R) (2011).

[14] M. Greiner, M. O. Mandel, T. Hänsch, and I. Bloch Nature **419**, 51 (2002).

[15] S. Will *et al.* Nature **465**, 197 (2010).

[16] P. R. Johnson, E. Tiesinga, J. V. Porto, and C. J. Williams, N. J. Phys. **11**, 093022 (2009).

[17] A. Smerzi, S. Fantoni, S. Giovanazzi, and R. S. Shenoy, Phys. Rev. Lett. **79**, 4950 (1997).

[18] D. Jaksch, C. Bruder, J. I. Cirac, C. W. Gardiner, and P. Zoller, Phys. Rev. Lett. **81**, 3108 (1998).

[19] C. Orzel *et al.*, Science **291**, 2386 (2001).

[20] A. Widera *et al.*, Phys. Rev. Lett. **100**, 140401 (2008).

[21] S. Fölling *et al.*, Nature **448**, 1029 (2007).

[22] K. Sakmann, A. I. Streltsov, O. E. Alon, and L. D. Cederbaum, Phys. Rev. Lett. **103**, 220601 (2009).

[23] D.-S. Lühmann, O. Jr̆gensen, and K. Sengstock, New J. Phys. **14**, 033021 (2012).

[24] T. Zibold, E. Nicklas, C. Gross, and M. K. Oberthaler, Phys. Rev. Lett. **105**, 204101 (2010).

[25] D. Cohen and R. Kottos, Phys. Rev. E **63**, 36203 (2001).